Understanding the role of atmospheric rivers in heavy precipitation in the Southeast US

Kelly Mahoney[1], Darren L. Jackson[2], Paul Neiman[1], Mimi Hughes[2], Lisa Darby[1],

Gary Wick[1], Allen White[1], Ellen Sukovich[2], Rob Cifelli[1]

[1]NOAA/Earth System Research Laboratory/Physical Sciences Division, Boulder, CO

[2]Cooperative Institute for Research in the Environmental Sciences/University of Colorado at Boulder/NOAA/ESRL, Boulder, CO

Corresponding author address:

Kelly M. Mahoney

NOAA/Earth System Research Laboratory

Physical Sciences Division

Mail Code R/PSD2; 325 Broadway

Boulder, Colorado 80305

Email: kelly.mahoney@noaa.gov

Submitted to:

Monthly Weather Review

10 August 2015

Revised:

29 January 2016

Abstract

An analysis of atmospheric rivers (ARs) as defined by an automated AR detection tool based on integrated water vapor transport (IVT) and the connection to heavy precipitation in Southeast U. S. (SEUS) is performed. Climatological water vapor and water vapor transport fields are compared between the U. S. West Coast (WCUS) and the SEUS, highlighting stronger seasonal variation in integrated water vapor in the SEUS, and stronger seasonal variation in IVT in the WCUS. The climatological analysis suggests that IVT values above ~500 kg m^{-1} s^{-1} (as incorporated into an objective identification tool such as the AR detection tool used here) may serve as a sensible threshold for defining ARs in the SEUS.

AR impacts on heavy precipitation in the SEUS are shown to vary on an annual cycle, and a connection between ARs and heavy precipitation during the non-summer months is demonstrated. When identified ARs are matched to heavy precipitation days (>100 mm day^{-1}), an average match rate of ~41% is found.

Results suggest that some aspects of an AR identification framework in the SEUS may offer benefit in forecasting heavy precipitation, particularly at medium-longer range forecast lead times. However, the relatively high frequency of SEUS heavy precipitation cases in which an AR is not identified necessitates additional careful consideration and incorporation of other critical aspects of heavy precipitation environments such that significant predictive skill might eventually result.

1. Introduction

1.1. Motivation

Many studies have documented the important role of atmospheric rivers (ARs) in producing extreme precipitation and flooding in the western U.S. (e.g., Neiman et al. 2008; Dettinger et al. 2011; Ralph and Dettinger 2012), however, relatively little research has been conducted on this topic in the Southeast U.S. Evidence suggests that some high-impact flood events in this region, such as the severe flooding in Tennessee in May 2010, have been partially driven by the presence of an AR (Moore et al. 2012; Lackmann 2013), but comprehensive understanding of the linkage between AR conditions and central/eastern U.S. precipitation remains undocumented. Part of the challenge in assessing the role of ARs in producing extreme precipitation is the very definition of AR conditions and the applicability of such a definition across different regions.

A recent extreme precipitation climatology produced as part of the NOAA Hydrometeorology Testbed (HMT) pilot project in the Southeast U.S. (HMT-SE) identified and categorized a collection of heavy precipitation cases and demonstrated that the causes of heavy precipitation in the Southeast United States (SEUS) are quite varied and diverse, but that some events may be linked to ARs (or AR-like features; Moore et al. 2015). In order to investigate the relevance of ARs in the SEUS, a newly-developed AR detection tool (ARDT; Wick 2014) based on vertically-integrated horizontal water vapor transport (IVT) is tested for the SEUS. ARs identified by the ARDT based on IVT are then compared with observed heavy precipitation events in order to quantify their relationship. In testing this identification tool and precipitation-matching technique we examine the applicability of an integrated water vapor (IWV)-based AR definition in a region outside of the

West Coast U.S. (WCUS) where the IWV-based AR definition was first developed (Ralph et al. 2004). We in turn consider how to account for the generally higher levels of background moisture and a more diverse array of precipitation generation mechanisms in the SEUS relative to the generally drier background environment and more orographically-focused precipitation found along the WCUS.

This manuscript will describe linkages between objectively-identified ARs and heavy precipitation events in the SEUS, as well as compare definitions and characteristics of ARs between the WCUS and SEUS. Our objectives in conducting this analysis are to: (i) examine how (and whether) ARs should be defined in the SEUS, (ii) compare definitions and characteristics of AR climatologies and precipitation linkages between the WCUS and SEUS, (iii) describe linkages between objectively-identified ARs and heavy precipitation events in the SEUS, and (iv) provide insight on whether defining synoptic-scale water vapor transport features as ARs in the SEUS provides any potential operational, applied, or research benefits to anticipating or understanding SEUS heavy precipitation events.

1.2. Previous research

Atmospheric rivers (ARs) are typically described as narrow, filamentary regions of enhanced water vapor transport, the presence of which has been observed to closely coincide with extreme precipitation and major flooding events along the west coast of North America, as well as many other regions around the globe (e.g., see Gimeno et al. 2014 and references therein). ARs are most often associated with moisture transport in the warm sector of mid-latitude cyclones. A number of studies have recently investigated the linkage between ARs (or features that can be related to ARs, e.g. warm conveyor belts, tropical moisture exports, etc.) and precipitation worldwide (Eckhardt et al. 2004; Knippertz and Martin 2007; Knippertz and Wernli 2010; Lavers and Villarini 2013; Neiman et al. 2013; Phfal et al. 2014; Rutz et al. 2014; Alexander et al. 2015; Lavers and Villarini 2015, and others).

WCUS-focused AR studies have found that ARs making landfall in California explain 20% - 50% of WCUS annual precipitation in the state (Dettinger et al. 2011), and that for some specific WCUS locations, nearly all extreme precipitation can be associated with landfalling ARs (e.g., Ralph and Dettinger 2012). Figure 1 summarizes results from previous studies which demonstrate that particularly high-intensity precipitation events (i.e., 72-h precipitation totals exceeding 500 mm) occur preferentially in both the SEUS and the WCUS regions of the United States, but the contribution of ARs to annual and extreme precipitation is best documented in the WCUS. The seasonality of heavy precipitation events in the western and eastern U.S. has also been shown to starkly differ, with cool (warm) season events being markedly more prominent in the western (eastern and central) U. S. (Fig. 1c; Ralph and Dettinger 2012).

ARs have been considered for their role in contributing to high-impact precipitation events in the SEUS as well. Moore et al. (2012) detail the role of an AR-like feature in supplying moisture to the 2010 Tennessee Floods. Moore et al. (2012) also point out how transport of water vapor from the tropics into the central and southeastern United States can occur in connection with ARs, but that due to the basic geography and associated synoptic-scale weather climatology of the North American continent (e.g., Hobbs et al. 1996), the processes associated with central and eastern

U.S. ARs likely differ in significant ways from those associated with “classic” pre-cold-frontal ARs over open-ocean basins. As such, the dynamical differences in which synoptic-scale cyclones are known to develop and impact the WCUS relative to the SEUS further motivates this work.

While there are certainly well-known, specific heavy precipitation cases featuring connections to ARs (or AR-like features, as described previously) in the SEUS, it is important to consider such events in a context recognizing that the SEUS experiences heavy precipitation events during all seasons and associated with a variety of atmospheric phenomena (e.g., Moore et al. 2015 and references therein). In contrast with the WCUS, corridors of strong water vapor transport (i.e., ARs or related terminologies) may extend from multiple different moisture source regions: the Gulf of Mexico, the Caribbean Sea, and the Atlantic Ocean (e.g., Pfahl et al. 2014). These corridors of water vapor transport provide moisture to areas of heavy precipitation produced in conjunction with a variety of potential precipitation triggering mechanisms [e.g., synoptic-scale frontal systems (e.g., Businger et al. 1990), land-falling tropical cyclones (e.g., Shepherd et al. 2007), mesoscale convective systems (e.g., Letkewicz and Parker 2010), orographic forcing along the Appalachian Mountains (e.g. Smith et al. 2011), and/or topographically-induced baroclinic zones (e.g. Koch and Ray 1997).] A number of previous studies have investigated various characteristics of heavy precipitation affecting the SEUS (e.g., Keim 1996; Konrad 1997, 2001; Brooks and Stensrud 2000; Schumacher and Johnson 2006; Mahoney and Lackmann 2007; Shepherd et al. 2007; Srock and Bosart 2009; Moore et al. 2015, and others), but none to our knowledge have focused on the specific role that ARs may play in the region’s complex heavy precipitation climatology.

2. Data and methods

Past studies have established criteria for the visual identification of ARs based on fields of integrated water vapor (IWV) from either satellite retrievals (e.g., Neiman et al. 2008; Wick et al. 2013a) or numerical weather prediction (NWP) models (e.g., Lavers and Villarini 2013; Wick et al. 2013b; Rutz et al. 2014). In order to make AR identification both automated and objective, an Atmospheric River Detection Tool (ARDT; Wick et al. 2013a) was developed based on thresholds of width, length, and IWV content of a given enhanced-IWV feature as informed by earlier, visual-identification-based studies. The ARDT based on IWV (ARDT-IWV) has been demonstrated to agree remarkably well with visual identification of ARs on the WCUS, as well as to be successful in reproducing climatologies of landfalling AR events. It has also been employed in evaluating the ability of NWP models to forecast the characteristics and landfall of ARs along the west coast of North America (Wick et al. 2013b).

While highly valued for its ability to be employed on fields directly available from satellite retrievals, the ARDT-IWV does not address the water vapor transport that most directly characterizes an AR. An enhanced version of the ARDT has now been developed for application to fields of IVT (i.e., ARDT-IVT) derived from NWP models and reanalyses. This enhancement further invokes the river analogy by accounting for the speed of the flow (wind), imposing a new requirement that the IVT be aligned with the primary axis of the feature itself, and thus better distinguishes the moisture transport corridor in environments of large background moisture, such as the SEUS. Figure 2 illustrates fields of IWV and IVT for two different extreme precipitation events: one in which the differences in feature identification are slight (3 May 2010; Fig. 2a, c) and one in which large background moisture highlights visually an advantage of using IVT to identify the moisture transport feature (22 September 2003; Fig. 2b, d). Daily accumulated precipitation in both cases corresponds closely to the points identified by the ARDT-IVT (Fig. 2e, f). For additional details regarding the design, implementation, and initial evaluation of the ARDT-IVT, the reader is pointed to Wick et al. (2016).

For this study, the ARDT-IVT was applied to the NCEP Climate Forecast System Reanalysis (CFSR; Saha et al. 2010) for the period January 2002 – April 2014. The CFSR, produced at T382L64 spectral resolution (~38 km), was obtained on a 0.5° latitude × 0.5° longitude global grid with 37 isobaric levels at 6-h temporal resolution. The ARDT-IVT employed a minimum IVT threshold of 500 kg m^{-1} s^{-1} (for discussion of the basis for selecting this threshold see section 3), a maximum feature width of 1500 km, and a minimum length of 1500 km. The ARDT-IVT produces a number of output variables that are useful for analysis, including time, location, IVT, AR width, and AR orientation angle. Location is defined by axis points along the length of the AR, and IVT, width, and angle of AR axis orientation are provided at each axis point.

In order to match identified ARs with heavy precipitation events, the Livneh et al. (2013) precipitation dataset was analyzed over the SEUS region (31°N – 39°N, 90°W – 75°W) from January 2002 – December 2011. The Livneh et al. (2013) dataset documents daily precipitation on a 1/16° grid based on approximately 20,000 NOAA cooperative observer (COOP) stations. Heavy daily precipitation was defined using gridpoint values in excess of 100 mm day^{-1}. Mean event locations for each event were computed using all heavy precipitation gridpoints for a given day; gridpoints that occurred outside of a 2° standard deviation of latitude and longitude from the computed mean location were eliminated in order to consolidate geographical areas and thus focus on coherent regions of precipitation. After this screening procedure, 249 heavy precipitation events were identified over the 2002 – 2011 period. These events very closely match those identified by analyzing the radar-based Stage IV precipitation dataset in Moore et al. (2015), demonstrating the fidelity of the precipitation event identification process in both studies. A portion of these events were further subset into a “larger-spatial scale” heavy precipitation event category by establishing a size requirement based on the 90th percentile of the number of gridpoints exceeding the heavy threshold across the 249 identified events. Thus, the resulting 25 “larger-spatial scale” heavy precipitation events all possessed greater than 171 gridpoints (~7000 km^2) in which precipitation exceeded 100 mm day^{-1}.

Once ARs and heavy precipitation events were identified, the matching of heavy precipitation events and ARs was defined by evaluating various space- and time-matching criteria. While several matching criteria were evaluated, the two used in this study are: (i) the minimum distance between a precipitation event’s average center point and at least one AR axis location must be less than 250 km; and (ii) the heavy precipitation event must have occurred within a 24-hour period of AR identification. The rationale for selecting these specific criteria is further discussed in the following section.

Finally, numerical model quantitative precipitation forecast (QPF) skill for AR-matched events (i.e., heavy precipitation events found to be associated with an identified AR) and AR-unmatched events (i.e., heavy precipitation events *not* found to be associated with an identified AR) was assessed for the NOAA second-generation Global Ensemble Forecast System (GEFS) reforecast dataset (Hamill et al. 2013) following the same methods used in Moore et al. (2015). The GEFS reforecast dataset is an archive (1985 – present) of 0 – 16-day global ensemble forecasts initialized daily using a fixed model configuration consistent with the 2012–14 version of the operational NCEP GEFS. The "fixed" status of the dataset allows one to evaluate forecast performance over an extended period of time without having to account for changes in operational modeling systems.

3. IWV and IVT climatological comparison between the western and southeast U.S.

WCUS ARs have been defined in many past studies using IWV as the main metric of identification (e.g., Neiman et al. 2008, and many others); however, originally (Newell et al. 1992; Zhu and Newell 1998) and again more recently IVT has also been used to identify ARs (e.g., Moore et al. 2012; Lavers and Villarini 2013; Rutz et al. 2014; Wick et al. 2016, and others). How (and perhaps whether) one should define an AR in the SEUS is itself a relatively complex question. Identification based on water vapor versus water vapor transport (e.g., Fig. 2), and the need to account for the larger background IWV values in the SEUS relative to the WCUS, present questions with respect to how to appropriately and most effectively identify AR features in this region.

Building on previously-discussed WCUS work, we first compare climatologies of IWV and IVT between the SEUS and WCUS regions to identify salient regional differences in moisture and moisture transport using the CFSR (Fig. 3). Monthly IWV and IVT percentiles are calculated at each grid point and are averaged within a Pacific region and a SEUS region that includes portions of both the Gulf of Mexico and the Atlantic Ocean (see boxes in Fig. 4). Though all area-averaged IWV percentiles (50^{th} – 99^{th}) peak during the warm season in both regions, a markedly stronger seasonal variation is clear in the SEUS (Fig. 3). The annual average for all percentiles also tends to be larger in the SEUS.

The area-averaged climatological IVT percentiles differ in several ways from the IWV percentiles: in the SEUS, most IVT percentiles are relatively steady throughout the year (with a notable exception of a September peak in the 95th percentile, which aligns with the climatological peak of tropical cyclone activity), illustrating a negative correlation between water vapor (more moist in the warm season) and kinematic forcing (stronger in the cool season). In contrast, there is a noticeable annual cycle in IVT in WCUS domain, with the largest transports occurring in the cool season. Additionally, IVT decreases more markedly from the cold season to the warm season at higher percentiles of IVT in the Pacific region relative to the SEUS, showing the shortage of transient mid-latitude baroclinic disturbances affecting this region during the summer months (Fig. 3). Such regional differences are rather stark even considering that the Pacific region averages mostly over the upstream (Pacific Ocean) moisture region, but by virtue of geography, the SEUS region includes a large area over land as well. Comparing maps of upper (95th) percentiles of IWV and IVT across cool (e.g, January) and warm (e.g., July) months again underscores the advantage of using IVT to characterize ARs in the warm season in the SEUS in particular, where warm-season background values of IWV are comparable to those found at Tropical latitudes (Fig. 4.)

In addition to the comparison of percentile-based regional IWV and IVT climatologies, a SEUS-specific analysis of IWV and IVT based on heavy precipitation events identified in Moore et al. (2015) demonstrates a very poor correlation of IWV and IVT themselves during heavy precipitation events (Fig. 5, and Moore et al. (2015)). Furthermore, the relationship between IWV, IVT, and precipitation amount also reveals no significant correlation, and further demonstrates that SEUS heavy precipitation events can still occur when IVT is relatively weak. This additional analysis (featuring both an independent precipitation event dataset and characterization of IWV and IVT) further underscores differences between the SEUS and WCUS, the latter of which possesses a very strong IWV-IVT correlation (e.g., Ralph et al. 2004; 2011; Neiman et al. 2014). [Though due to the inclusion of storm kinematic processes which focus moisture transport, advantages of IVT over IWV have been recently demonstrated for the WCUS (and other regions) as well (see Wick et al. 2016).] While past studies of ARs over the Pacific Ocean and the WCUS have used 250 kg m^{-1} s^{-1} as an IVT threshold (e.g., Rutz et al. 2014; 2015), based on this comparative climatological analysis, we elect to use a threshold of 500 kg m^{-1} s^{-1} with the intent to identify the strongest systems that would be most likely to affect large-scale heavy precipitation in the SEUS. A threshold of 500 kg m^{-1} s^{-1} falls approximately between the 90 – 95th percentiles of SEUS monthly average IVT values (Fig. 3c).

Changing the threshold from 500 kg m^{-1} s^{-1} to 250 kg m^{-1} s^{-1} results in a roughly 80% increase in the number of gridpoints and times identified as having an AR present. Use of the lower threshold significantly increases the number of potential AR events found to not correspond to extreme precipitation. Recent NOAA Hydrometeorology Testbed experience in the WCUS interacting with National Weather Service forecasters and other stakeholders also suggests that the 250 kg m^{-1} s^{-1} threshold is too low to be useful in identifying the most significant precipitation threats associated with ARs. Use of the 500 kg m^{-1} s^{-1} threshold has been chosen to focus on identification of the most hydrologically significant events and is now also being employed in a suite of real-time AR forecast diagnostics over the entire CONUS, presently used by forecasters at the NOAA Weather Prediction Center. The results are also sensitive to the specific length and width criteria employed, but not to the degree of the primary IVT threshold. Changing the length and width criteria thus impacts the number of detected ARs, but does not significantly change the primary conclusions of this study. A detailed analysis of the sensitivity of identified AR events to the ARDT thresholds and identification criteria will be contained in Wick et al. (2016).

These regional moisture parameter comparisons illustrate several compelling reasons to define SEUS ARs by water vapor transport instead of solely by water vapor, particularly if the purpose is to identify storm systems with strong kinematic forcing from environments that may be moisture-rich but are not dominated by dynamics. This choice also acknowledges that we are interested in storms whose internal dynamics contribute to precipitation production (e.g., synoptic-scale frontal systems, tropical cyclones, mesoscale convective systems) rather than precipitation depending on external triggering mechanisms (e.g., topography). The necessity of carefully considering IWV versus IVT and various associated threshold values to account for kinematic forcing relative to a moist background state is in considerable contrast to the WCUS, where mountains generally act as static orographic termini that can directly force precipitation given adequate moisture convergence and favorable winds. Though the dynamics of the very system transporting the water vapor are of critical importance regardless of region, the SEUS is known to feature a highly variable array of precipitation triggering mechanisms (e.g., Moore et al. 2015), in which direct orographic influence from the Appalachian Mountains affects a relatively small fraction of events observed across the larger region of interest.

4. Connection between SEUS ARs and heavy precipitation

4.1 Sensitivity to AR matching criteria and seasonality of AR-matched events

With a working definition of a SEUS AR established, the next step is to connect defined ARs with observed heavy precipitation events. As described in section 2, a “match” occurs between a given AR and an associated heavy precipitation event if at least one AR axis point is located within a 250-km radius of a heavy precipitation point and occurs within the same 24-hour period. However, it is important to show that describing the degree of linkage between the 249 heavy precipitation events (identified as described in section 2) to ARs is understandably sensitive to such imposed requirements. Figure 6 shows this relationship as a function of space and time criteria; the highest rate of matching (i.e., AR-associated heavy precipitation events; 63%) occurs when matching criteria is most flexible, allowing ARs and heavy precipitation events to be separated by up to 500 km and occur within a common 48-hour period. Lower rates of AR-heavy-precipitation event matching occurs when criteria become more restrictive: e.g., a matching distance allowance threshold of 100 km and a time period restriction of 24 hours yields a match rate of just 29%. To best fit the space- and time- scales in which we are most interested (i.e., daily precipitation associated with a single synoptic weather system), we adopt the criteria that at least one AR point be located within a 250-km radius of a heavy precipitation point and occur within the same 24-hour period. This definition yields an average match rate of ~41% [i.e., 41% (102 events) of the identified 249 heavy precipitation events are matched with an identified AR.]

Having established an AR/heavy-precipitation matching definition, the seasonality and salient features of AR-associated heavy precipitation events can be described. On an annual cycle, while SEUS heavy precipitation events peak in the warm season (May – Oct; Fig. 7a), AR- and heavy precipitation event matches tend to peak in the cool season and transition months, with a notable minimum in July and August in particular (Fig. 7b). These results likely reflect the combined effects of the SEUS warm season peak in IWV, relative decrease in synoptic-scale dynamic forcing, and dominance of small-scale convection, and the finding is quite consistent with many past studies of SEUS precipitation patterns (including Moore et al. (2015) and others.) Climatological and physical characteristics of all identified AR events reveal some differences between ARs that are matched with a heavy precipitation event versus those that are not. Matched events have a mean IVT of 853 kg m^{-1} s^{-1} relative to 759 kg m^{-1} s^{-1} for unmatched AR events. The width of AR features is on average 854 km and 584 km for matched and unmatched AR events, respectively. Thus, for most months of the year, both AR intensity and width tend to be greater in events matched with heavy precipitation (Fig. 8).

The seasonal distribution of matched events also reveals a few notable geographic trends (Fig. 9). Winter (DJF) and spring (MAM) events most commonly occur in the western portion of the SEUS domain, suggesting the influence of strong synoptic weather systems transporting water vapor from the Gulf of Mexico during these months (e.g., Mahoney and Lackmann 2007; Moore et al. 2015). There is a more general and varied distribution of summer (JJA) events slightly favoring southern and eastern locations within the SEUS domain. Multiple fall (SON) matched event clusters are also evident, such as in western North Carolina near the Appalachian Mountain foothills and eastern North Carolina (hinting at the possible role of landfalling tropical systems; see Brun and Barros (2014) and further analysis below), and in the far western portion of the domain as Gulf of Mexico moisture is again tapped by stronger synoptic systems in the fall season months. Small-to-moderate sized matched events (1 – 500 gridpoints) occur in all seasons, while only the spring and fall transition seasons show large-scale events (501 – 1500 gridpoints). Fall has the greatest number of large-scale events (likely due to the influence of tropical systems), and summer has the most small-scale events, suggesting the dominance of less-organized, convective modes of precipitation. Many of these results are also in qualitative agreement with recent studies such as Lavers and Villarini (2015), which examine the role of ARs across Europe and the United States and find similar seasonality and levels of AR attribution in the SEUS.

4.2 Larger-spatial scale heavy precipitation events and connection to tropical systems

As ARs and the systems that drive them are generally large- (synoptic-) scale features, “larger-spatial scale” heavy precipitation events are also separately analyzed in order to determine to what extent there exists a preferential connection between ARs and larger-scale heavy precipitation events. Considering heavy precipitation events of all sizes, events matched with ARs are larger on average than those without (an average of 91 gridpoints or ~3700 km^2 for AR-matched events vs. 61 gridpoints or ~2500 km^2 for events not matched with an AR.) Because larger-spatial scale precipitation events may affect more people and property (depending on where they occur), and thus be of potentially greater societal impact, a focus on this larger-spatial scale event subset is of particular interest. Figure 7b illustrates that larger-spatial scale heavy precipitation events (defined in section 2 to be those events in which greater than 171 gridpoints (~7000 km^2) exceed 100 mm day^{-1}) are also more often matched with ARs than smaller-scale events; ~52% (13 events) of all of the 25 larger-spatial scale heavy precipitation events identified in the precipitation climatology are matched with identified ARs within 250-km and 24-h. This relationship is strongest during the cool season months (October – May; not shown due to small sample sizes in some months).

It is also of potential significance that of the 25 larger-spatial scale heavy precipitation events identified, 18 were tropical in origin (i.e., linked with a system that began as a named tropical cyclone (TC) according to the National Hurricane Center's Hurricane Database (HURDAT) reanalysis). Of these 18 tropical system-linked, large-scale heavy precipitation events, 10 events had ARs identified by the ARDT-IVT during or immediately following the extratropical transition (ET; Jones et al. 2003)) process. One example of such an occurrence was during the ET of Tropical Storm Nicole (2010) (Fig. 10), in which the interaction of TS Nicole and a mid-latitude trough resulted in over 500 mm (~20 inches) of rain in parts of North Carolina over a five-day period. The linear feature identified by the objective ARDT-IVT algorithm shows clearly the uninterrupted connection to the Caribbean Sea moisture source during this period (Fig. 10b,c). A relatively steady conduit of deep, tropical moisture was indeed evident and identified by the ARDT in all 10 of the larger-spatial scale heavy precipitation events that exhibited both an original TC connection and an identified AR. The AR framework may thus offer a means to track and display a traceable, objectively-detectable mechanism for sustained infusion of water vapor capable of fueling the intense and often long-duration precipitation associated with some ET systems.

Recent studies have demonstrated that heavy rainfall produced by extratropical-transitioning TCs can be produced by a variety of related, but distinguishable mechanisms ranging from precipitation stemming from the transitioning TC itself to precipitation displaced well poleward of the TC, as is the case in predecessor rain events (PREs; Galarneau et al. 2010; Moore et al. 2013) -- the latter of which also describes the precipitation associated with the ET of TS Nicole discussed above. This potential TC connection presents another difference between SEUS and WCUS ARs: while connections of North Pacific TCs to ARs in the ET transition process have been shown

(Cordeira et al. 2013; Knippertz et al. 2013), this is not necessarily an oft-considered (or at least not a well-documented) part of the Pacific AR climatology. The exploratory analysis performed here only scratches the surface of this question as it relates to SEUS heavy precipitation, but suggests that the connection of ARs, transitioning TCs, and larger-spatial scale heavy precipitation events may be a noteworthy aspect of the AR-precipitation climatology in this region, and may offer a framework useful for defining and tracking sustained, linear connections between mid-latitude heavy precipitation events and tropical moisture reservoirs.

4.3 Precipitation events unassociated with ARs

If the identification of ARs in the SEUS is undertaken in the context of evaluating its potential utility in forecasting heavy precipitation, then we should also consider situations in which (a) an AR is identified but heavy precipitation does not result and (b) heavy precipitation is produced in the absence of a defined AR. As such, in order to understand connections between SEUS ARs and low, moderate, and high precipitation rate events, we slightly modify the matching technique described in section 2. A proxy for low, moderate, and high precipitation rates in the SEUS region is created by first defining a regional daily maximum precipitation threshold as the mean of the highest ten daily precipitation gridpoint values from the Livneh et al. (2013) data set for a given day over the entire SEUS domain. The distribution over the 10-year period of these daily maximum precipitation mean values enables definition of a spectrum of regional daily precipitation rate intensities: lower-intensity rates below the 5th percentile (6.66 mm/day), moderate-intensity rates around the 50th percentile (37.96 mm/day), and higher-intensity rates above the 95th percentile

(98.74 mm/day). We then assess the impact that identified ARs may have on these precipitation thresholds for the SEUS region by identifying the percentage of daily AR detections associated with days above and below each percentile level. AR detections are defined here by the identification of at least one axis point by the ARDT-IVT anywhere within the detection region and within the 24-hour precipitation period. Note that as no direct matching of ARs to the precipitation location was done for this more general regional assessment, this particular means of analysis does not guarantee a direct physical link to the precipitation in SEUS region but rather seeks to define a more general level of potential impact of an AR-producing environment.

Figure 11 shows percentages of region-wide AR detection occurring in precipitation events above or below the 5th, 50th, and 95th percentile levels. The plot shows a general increase in AR detection percentage for higher precipitation days: the percentage of AR detections for precipitation days above the 95th percentile is 61%. The percentage of AR detections in the SEUS region for the lowest precipitation days (below the 5th percentile) is just 2%. While AR conditions are obviously more likely to occur in the SEUS region on days when heavy precipitation occurs, this analysis clearly demonstrates the degree to which the presence of an AR is not a necessary condition. [However, the 25 – 30% difference in the AR detection percentage above and below each percentile level shows a significant AR influence on higher precipitation rates and is indeed greatest for the heaviest (95th percentile) precipitation events.] The 61% detection rate shown above is also significantly lower than that observed for WCUS ARs associated with extreme precipitation (Ralph and Dettinger 2012) but higher than the ~41% detection rate discussed previously using more stringent, direct matching of ARs with precipitation events. This further suggests that AR conditions in the SEUS may frequently have a less direct influence on heavy precipitation (e.g., instead "priming" the larger-scale environment by supplying ample background moisture, or simply being too transient to have a definitively-linked effect on precipitation), and may be often secondary to the many other potential forcing mechanisms known to produce heavy rainfall in this region.

Seasonal variation of the regional AR detection percentages across various precipitation intensity thresholds sheds further light on the association of ARs with winter extratropical storms and the lesser influence of ARs on high precipitation rates produced by smaller-scale warm season convection. Figure 11b shows a monthly climatology of AR detection percentages above the 95th percentile and below the 5th percentile. For high precipitation rate cases exceeding the 95th percentile, AR detection percentage is generally ~60% or higher, with notable exceptions in July, August, and September, during which the detection rate reduces to less than 50%. Therefore, the 61% annual rate of detection above the 95th percentile is reduced significantly by a decrease in detection rates during the summer when localized convection and landfalling tropical storms (e.g., those in which the TC itself produces the rainfall and never forms an ARDT-IVT detectable feature) are more likely to produce heavy precipitation.

Regarding identified ARs that are *not* associated with significant precipitation, AR detections on the lowest precipitation days (below the 5th percentile) occur only four times in our analysis period. All four instances occur in either February or October, and all are associated with mature extratropical storms in which the high precipitation rates have exited the SEUS domain and moved over the Atlantic Ocean [i.e., where no data exists in the Livneh et al. (2013) dataset], but where the southwestern region of the AR still intersects a portion of the SEUS region. Therefore, while ARs (as defined herein) are indeed identified on a significant percentage of non-"extreme" days (i.e., <100 mm day^{-1}), we find little-to-no evidence of cases in which an AR is detected by our algorithm but does not produce precipitation equal to or greater than the 5th percentile day values, or ~6.66 mm day^{-1}, somewhere in the SEUS region.

Finally, as discussed in section 1, it is well known that the SEUS features a diverse portfolio of heavy precipitation triggering mechanisms and event types. It is beyond the scope of this study to further characterize or classify heavy precipitation events that are not linked to ARs, and the reader is encouraged to consult the significant body of literature that already exists on precipitation in the SEUS [including Moore et al. (2015) and references therein.]

5. Predictive skill of AR-matched and AR-unmatched heavy precipitation cases

Based on prior research demonstrating increased forecast skill in environments characterized by strong synoptic-scale forcing (e.g., Stensrud and Fritsch 1994; Jankov and Gallus 2004; Hohenegger et al. 2006; Schumacher and Davis 2010; Moore et al. 2015) and the degree of synoptic-scale forcing that characterizes most AR-matched events, we hypothesize that numerical model QPF skill is generally greater for heavy precipitation events that are matched with ARs relative to those events that are not matched to an AR feature. To test this hypothesis, we use the method of Moore et al. (2015) to inspect deterministic 24-h precipitation accumulation forecasts from the GEFS reforecast control member at 12-h – 132-h lead times for the 30 heaviest precipitation events matched with ARs and the 30 heaviest precipitation cases without matched ARs. Equitable threat score (ETS; Schaefer 1990) and multiplicative bias (BIA; Wilks 2011) are evaluated.

Confirming our hypothesis, an ETS analysis (Fig. 12a) reveals greater skill at all lead times for a moderately heavy (>40-mm/24h; following Moore et al. 2015) category of precipitation events that were matched with ARs relative to cases in which no identified AR was linked. The difference in skill between the two event categories is relatively consistent across forecast lead times, with ETS for the AR-matched events remaining consistently higher than non-AR-matched events even as skill in both event categories decreases steadily with time. Consistent with the relative differences in the ETS between the two categories, as well as with the general results found in Moore et al. (2015) for events separated according to IVT strength, BIA values for the AR-matched category are less (i.e., closer to one) than those for the non-AR-matched category at precipitation amounts above 40 mm (Fig. 12b). The brief analysis performed here is not intended to be exhaustive but is included to demonstrate a type of QPF verification analysis that could be further undertaken to more specifically identify forecast challenges and improvement opportunities for AR- or non-AR-matched events.

6. Conclusions

An analysis of ARs as defined by an automated detection tool based on integrated water vapor transport and the connection to heavy precipitation in the SEUS is performed. Climatological IWV and IVT fields are compared between the WCUS and the SEUS, highlighting stronger seasonal variation in IWV in the SEUS, and stronger seasonal variation in IVT in the WCUS. The climatological analysis suggests that IVT values above ~500 kg m^{-1} s^{-1} (as incorporated into an objective identification framework provided by the ARDT-IVT) serves as a sensible threshold for defining ARs in the SEUS.

AR impacts on heavy precipitation in the SEUS are shown here to vary throughout the year, and a reasonably clear connection between ARs and heavy precipitation during the non-summer months is demonstrated. When identified ARs are matched to heavy precipitation days [gridpoint values >100 mm day^{-1} in the Livneh et al. (2013) precipitation dataset] according to the constraint that at least one AR point be located within a250-km radius of a heavy precipitation point and occur within the same 24-hour period, an average match rate of ~41% is found. ARs matched to heavy precipitation were found to have a larger mean IVT and AR width then ARs not associated with heavy precipitation.

Larger-spatial scale heavy precipitation events (in which greater than 171 gridpoints (~7000 km^2) in the SEUS domain exceed 100 mm day^{-1}) are matched with ARs at a rate of 52% over the course of the year, with a slight increase in matching rates occurring in cool/transition season months (October – May) when both large-scale moisture and synoptically-driven transport mechanisms are relatively common. A significant portion of larger-spatial scale heavy precipitation events linked with ARs were also associated with a TC (i.e., originated from a named TC according the National Hurricane Center). The connection to tropical moisture via tropical-extra-tropical transitions is also a notable departure from the usual characteristics of WCUS ARs, and as such, may present new criteria that future research – as well as future versions of the ARDT-IVT – may wish to consider.

Two types of unmatched AR/precipitation cases are also briefly considered: (a) identified ARs that do not result in particularly heavy precipitation, and (b) heavy precipitation events unassociated with an AR. With respect to (a), an analysis of regional light-, moderate-, and heavy- precipitation days shows that while AR conditions are more likely to occur in the SEUS region on days when heavy precipitation occurs relative to days when only moderate or light precipitation occurs, it is not a necessary condition. Furthermore, we find little-to-no evidence of cases in which an AR is detected by our algorithm but measurable precipitation (>~6.66 mm day^{-1}) is not found somewhere in the SEUS. With respect to the 60% of heavy precipitation events unassociated with ARs, these are likely better described in terms of other forcing mechanisms (e.g., mesoscale convective systems, orographic forcing, baroclinic boundary interactions), many of which are thoroughly investigated by previous studies. Overall, results suggest that AR conditions in the SEUS may frequently have an influence – but a decidedly *less direct* influence relative to the WCUS - on heavy precipitation. In other words, it is likely that ARs or AR-like-features often "prime" the larger-scale environment but may be secondary to the many other potential forcing mechanisms known to produce heavy rainfall in this region.

A precursory comparison of forecast performance metrics for heavy precipitation events with and without associated ARs suggests that there is a slight increase in forecast skill and decrease in bias for areas of heavy precipitation with an associated AR. While it is beyond the scope of this study to systematically assess precipitation forecast skill in AR vs. non-AR environments, the rudimentary analysis included here indicates that using a tool such as the ARDT-IVT may be one way to increase forecaster situational awareness at extended lead times and take better advantage of the generally more inherently-predictable large-scale atmospheric patterns most often associated with identified ARs.

Certain aspects of the study findings thus suggest that the AR framework in the SEUS may offer QPF improvement opportunities. The qualitative analysis of ARs identified during ET events, as well as related recent work on tropical moisture exports (Knippertz and Wernli 2010; Knippertz et al. 2013) suggests utility in defining and tracking sustained, linear connections between mid-latitude heavy precipitation potential and tropical moisture reservoirs associated with TCs. Though an AR-tropical connection may not yield forecast utility in isolation, the relationship suggests that identifying specific water vapor transport features that provide continuous tropical moisture transport during the ET process may help identify environments conducive to exceptionally heavy rainfall. In addition to the possible connection to the ET process of TCs, there is work ongoing to create AR diagnostics which account for the temporal persistence of AR-like features, particularly at the mid- to extended range forecast periods. Moore et al. (2012) in particular highlight the importance of a relatively static or stationary atmospheric connection supplying the SEUS midlatitude environment with moisture from a low-latitude moisture reservoir, and as such, this idea is the basis for ongoing research and testing. Finally, however, the relatively high frequency of heavy precipitation cases in which an AR is not identified (or is not closely enough matched in space and time) necessitates additional research to more reliably connect identified ARs with other critical aspects of heavy precipitation environments such that a significant increase in predictive skill may potentially result.

Acknowledgements

We gratefully acknowledge support from the Hurricane Sandy Supplemental Funding Award NA14OAR4830066, the United States Weather Research Program – Hydrometeorology Testbed, and NOAA ESRL Physical Sciences Division. We also value the helpful input from three anonymous reviewers, as well as the collaboration of Benjamin Moore (SUNY-Albany), Tom Hamill (NOAA ESRL PSD), Michael Brennan (NOAA National Hurricane Center) ,and Sarah Perfator, Ben Albrecht, and David Novak (NOAA NCEP Weather Prediction Center).

References

Alexander, M. A., J. D. Scott, D. Swales, M. Hughes, K. Mahoney, and C. A. Smith, 2015: Moisture pathways into the U.S. Intermountain West associated with heavy winter precipitation events. *J. Hydrometeor*, **16**, 1184–1206.

Brooks, H. E., and D. J. Stensrud, 2000: Climatology of heavy rain events in the United States from hourly precipitation observations. *Mon. Wea. Rev.*, **128**, 1194–1201.

Brun, J, and Barros, A. P., 2014: Mapping the role of tropical cyclones on the hydroclimate of the southeast United States: 2002-2011. International Journal of Climatology, **34,** 494- 517.

Businger, S., D. I. Knapp, and G. F. Watson, 1990: Storm following climatology of precipitation associated with winter cyclones originating over the Gulf of Mexico. *Wea. Forecasting*, **5**, 378–403,

Cordeira, J. M. , F. M. Ralph, and B. J. Moore, 2013: The development and evolution of two atmospheric rivers in proximity to western North Pacific tropical cyclones in October 2010. *Mon. Wea. Rev.*, **141**, 4234–4255.

Dettinger, M. D., F. M. Ralph, T. Das, P. J. Neiman, and D. Cayan, 2011: Atmospheric rivers, floods, and the water resources of California. *Water*, **3**, 455–478.

Eckhardt, S., A. Stohl, H. Wernli, P. James, C. Forster, and N. Spichtinger, 2004: A 15-year climatology of warm conveyor belts. *J. Climate*, **17**, 218–237.

Galarneau, T. J. Jr., L. F. Bosart, and R. S. Schumacher, 2010: Predecessor rain events ahead of tropical cyclones. *Mon. Wea. Rev.*, **138**, 3272–3297. doi: http://dx.doi.org/10.1175/2010MWR3243.1

Gimeno, L., Nieto, R., Vázquez, M., Lavers, D. A., 2014: Atmospheric rivers: a mini-review. Frontiers in Earth Science, 2, DOI=10.3389/feart.2014.00002

Hamill, T. M., 2012: Verification of TIGGE multimodel and ECMWF reforecast-calibrated probabilistic precipitation forecasts over the contiguous United States. *Mon. Wea. Rev.*, **140**, 2232–2252.

Hamill, T. M., G. T. Bates, J. S. Whitaker, D. R. Murray, M. Fiorino, T. J. Galarneau Jr., Y. Zhu, and W. Lapenta, 2013: NOAA's second-generation global medium-range ensemble reforecast dataset. *Bull. Amer. Meteor. Soc.*, **94**, 1553–1565, doi:10.1175/BAMS-D-12-00014.1.

Higgins, R. W., J. E. Janowiak, and Y.-P. Yao, 1996: A gridded hourly precipitation data base for the United States (1963–1993). *NCEP/Climate Prediction Center Atlas 1,* U.S. Department of Commerce, NOAA/NSW, 47 pp.

Hohenegger, C., D. Lüthi, and C. Schär, 2006: Predictability mysteries in cloud-resolving models. *Mon. Wea. Rev.*, **134**, 2095–2107, doi:10.1175/MWR3176.1

Hou, D., and Coauthors, 2014: Climatology-calibrated precipitation analysis at fine scales: Statistical adjustment of stage IV toward CPC gauge-based analysis. *J. Hydrometeor.*, **15**, 2542–2557.

Jankov, I., and W. A. Gallus Jr., 2004: MCS rainfall forecast accuracy as a function of large-scale forcing. *Wea. Forecasting*, **19**, 428–439.

Jones, S. C., P. A. Harr, J. Abraham, L. F. Bosart, P. J. Bowyer, J. L. Evans, D. E. Hanley, B. N. Hanstrum, R. E. Hart, F. Lalaurette, M. R. Sinclair, R. K. Smith and C. Thorncroft. 2003: The extratropical transition of tropical cyclones: Forecast challenges, current understanding, and future directions. *Wea. Forecasting*, **18**, 1052–1092.

Keim, B. D., 1996: Spatial, synoptic, and seasonal patterns of heavy rainfall in the southeastern United States. *Phys. Geogr.*, **17**, 313–328, doi:10.1080/02723646.1996.10642588.

Knippertz, P., and J. E. Martin, 2007: A Pacific moisture conveyor belt and its relationship to a significant precipitation event in the semiarid southwestern United States. *Wea. Forecasting*, **22**, 125–144.

Knippertz, P., and H. Wernli, 2010: A Lagrangian climatology of tropical moisture exports to the Northern Hemispheric extratropics. *J. Climate*, **23**, 987–1003.

Knippertz, P., H. Wernli, and G. Gläser, 2013: A global climatology of tropical moisture exports. *J. Climate*, **26**, 3031–3045.

Koch, S. E., and C. A. Ray, 1997: Mesoanalysis of summertime convergence zones in central and eastern North Carolina. *Wea. Forecasting*, **12**, 56–77, doi:10.1175/1520-0434(1997)012<0056:MOSCZI>2.0.CO;2.

Konrad, C. E., II, 1997: Synoptic-scale features associated with warm season heavy rainfall over the interior southeastern United States. *Wea. Forecasting*, **12**, 557–571.

Konrad, C. E., II, 2001: The most extreme precipitation events over the eastern United States from 1950 to 1996: Considerations of scale. *J. Hydrometeor.*, **2**, 309–325.

Lackmann, G. M., 2013: The south-central U.S. flood of May 2010: Present and future. *J. Climate*, **26**, 4688–4709.

Lavers, D. A., and G. Villarini, 2013: Atmospheric rivers and flooding over the central United States. *J. Climate*, **26**, 7829–7836.

Lavers, D. A., and G. Villarini, 2015: The contribution of atmospheric rivers to precipitation in Europe and the United States, *J. Hydrology, 522,* 382.

Letkewicz, C. E., and M. D. Parker, 2010: Forecasting the maintenance of mesoscale convective systems crossing the Appalachian Mountains. *Wea. Forecasting*, **25**, 1179–1195.

Livneh, B., E. A. Rosenberg, C. Lin, B. Nijssen, V. Mishra, K. M. Andreadis, E. P. Maurer, and D. P. Lettenmaier, 2013: A long-term hydrologically based dataset of land surface fluxes and states for the conterminous United States: Update and extensions. *J. Climate*, **26**, 9384–9392, doi:10.1175/JCLI-D-12-00508.1.

Mahoney, K. M., and G. M. Lackmann, 2007: The effects of upstream convection on downstream precipitation. *Wea. Forecasting*, **22**, 255–277, doi:10.1175/WAF986.1.

Moore, B. J., P. J. Neiman, F. M. Ralph, and F. E. Barthold, 2012: Physical processes associated with heavy flooding rainfall in Nashville, Tennessee, and vicinity during 1–2 May 2010: The role of an atmospheric river and mesoscale convective systems. *Mon. Wea. Rev.*, **140**, 358–378.

Moore, B. J., L. F. Bosart, D. Keyser, and M. L. Jurewicz, 2013: Synoptic-scale environments of predecessor rain events occurring east of the Rocky Mountains in association with Atlantic Basin tropical cyclones. *Mon. Wea. Rev.*, **141**, 1022–1047. doi: http://dx.doi.org/10.1175/MWR-D-12-00178.1

Moore, B. J., K. M. Mahoney, E. M. Sukovich, R. Cifelli, and T. M. Hamill, 2015: Climatology and environmental characteristics of extreme precipitation events in the Southeastern United States. *Mon. Wea. Rev.*, **143**, 718–741.

Neiman, P. J., F. M. Ralph, G. A. Wick, J. D. Lundquist, and M. D. Dettinger, 2008: Meteorological characteristics and overland precipitation impacts of atmospheric rivers affecting the west coast of North America based on eight years of SSM/I satellite observations. *J. Hydrometeor*, **9**, 22–47.

Neiman, P. J., L. J. Schick, F. M. Ralph, M. Hughes, and G. A. Wick, 2011: Flooding in western Washington: The connection to atmospheric rivers. *J. Hydrometeor.*, **12**, 1337–1358, doi: 10.1175/2011JHM1358.1.

Neiman, P. J., F. M. Ralph, B. J. Moore, M. Hughes, K. M. Mahoney, J. M. Cordeira, and M. D. Dettinger, 2013: The landfall and inland penetration of a flood-producing atmospheric river in Arizona. Part I: Observed synoptic-scale, orographic, and hydrometeorological characteristics. *J. Hydrometeor.*, **14**, 460–484, doi:10.1175/JHM-D-12-0101.1.

Neiman, P.J., G.A. Wick, B.J. Moore, F.M. Ralph, J.R. Spackman, and B. Ward, 2014: An airborne study of an atmospheric river over the subtropical Pacific during WISPAR: Dropsonde budget-box diagnostics, and precipitation impacts in Hawaii. *Mon. Wea. Rev.*, **142**, 3199-3223.

Newell, R. E., N. E. Newell, Y. Zhu, and C. Scott, 1992: Tropospheric rivers? – A pilot study. *Geophys. Res. Lett.*,**19,** 2401–2404.

Pfahl, S., E. Madonna, M. Boettcher, H. Joos, and H. Wernli, 2014: Warm conveyor belts in the ERA-Interim dataset (1979–2010). Part II: Moisture origin and relevance for precipitation. *J. Climate*, **27**, 27–40.

Ralph, F.M., P.J. Neiman, and G.A. Wick, 2004: Satellite and CALJET aircraft observations of atmospheric rivers over the eastern North-Pacific Ocean during the winter of 1997/98. *Mon. Wea. Rev.*, **132**, 1721-1745.

Ralph, F.M., P.J. Neiman, G.N. Kiladis, K. Weickmann, D.M. Reynolds, 2011: A multi-scale observational case study of a Pacific atmospheric river exhibiting tropical-extratropical connections and a mesoscale frontal wave. *Mon. Wea. Rev.*, **139**, 1169-1189.

Ralph, F.M. and M. D. Dettinger, 2012: Historical and national perspectives on extreme West Coast precipitation associated with atmospheric rivers during December 2010. *Bull. Amer. Meteor. Soc.*, **93**, 783–790.

Rutz, J. J., W. J. Steenburgh, and F. M. Ralph, 2014: Climatological characteristics of atmospheric rivers and their inland penetration over the western United States. *Mon. Wea. Rev.*, **142**, 905–921.

Rutz, J. J., W. J. Steenburgh, and F. M. Ralph, 2015: The Inland Penetration of Atmospheric Rivers over Western North America: A Lagrangian Analysis. *Mon. Wea. Rev.*, **143**, 1924–1944.

Saha, S., and Coauthors, 2010: The NCEP Climate Forecast System Reanalysis. *Bull. Amer. Meteor. Soc.*, **91**, 1015–1057, doi:10.1175/2010BAMS3001.1

Schumacher, R. S., and R. H. Johnson, 2006: Characteristics of U.S. extreme rain events during 1999–2003. *Wea. Forecasting*, **21**, 69–85, doi:10.1175/WAF900.1.

Schumacher, R. S., and C. A. Davis, 2010: Ensemble-based forecast uncertainty analysis of diverse heavy rainfall events. *Wea. Forecasting*, **25**, 1103–1122, doi:10.1175/2010WAF2222378.1.

Shepherd, J. M., A. Grundstein, and T. L. Mote, 2007: Quantifying the contribution of tropical cyclones to extreme rainfall along the coastal southeastern United States. *Geophys. Res. Lett.*, **34**, L23810, doi:10.1029/2007GL031694.

Smith, J. A. Smith, Mary Lynn Baeck, Alexandros A. Ntelekos, Gabriele Villarini, Matthias Steiner. (2011) Extreme rainfall and flooding from orographic thunderstorms in the central Appalachians. *Water Resources Research* **47.**

Srock, A. F., and L. F. Bosart, 2009: Heavy precipitation associated with southern Appalachian cold-air damming and Carolina coastal frontogenesis in advance of weak landfalling Tropical Storm Marco (1990). *Mon. Wea. Rev.*, **137**, 2448–2470, doi:10.1175/2009MWR2819.1.

Stensrud, D. J., and J. M. Fritsch, 1994: Mesoscale convective systems in weakly forced large-scale environments. Part III: Numerical simulations and implications for operational forecasting. *Mon. Wea. Rev.*, **122**, 2084–210

Sukovich, E. M., F. M. Ralph, F. E. Barthold, D. W. Reynolds, and D. R. Novak, 2014: Extreme quantitative precipitation forecast performance at the Weather Prediction Center from 2001 to 2011. *Wea. Forecasting*, **29**, 894–911, doi:10.1175/WAF-D-13-00061.1.

Wick, G. A., P. J. Neiman, and F. M. Ralph, 2013a: Description and validation of an automated objective technique for identification and characterization of the integrated water vapor signature of atmospheric rivers. *IEEE Trans. Geosci. Remote Sens.*, **51** (4), 2166–2176, doi:10.1109/TGRS.2012.2211024.

Wick, G. A., P. J. Neiman, F. M. Ralph, and T.M. Hamill, 2013b: Evaluation of forecasts of the water vapor signature of atmospheric rivers in operational numerical weather prediction models. *Wea. Forecasting*, **28**, 1337-1352, doi:10.1175/WAF-D-13-00025.1

Wick, G., 2014: Implementation and Initial Application of an Atmospheric River Detection Tool Based on Integrated Vapor Transport. AGU Annual Fall Meeting 2014, 17 December 2014.

Wick et al. 2016: Implementation and demonstration of an atmospheric river detection tool for integrated vapor transport. J. Atmos. Oceanic Tech., in preparation.

Zhu, Y., and R. E. Newell, 1998: A proposed algorithm for moisture fluxes from atmospheric rivers. *Mon. Wea. Rev.*, **126,** 725–735.

Figure Caption List

Figure 1. a) From Ralph and Dettinger (2012), their Fig. 3: Maximum 3-day precipitation totals at 5,877 COOP stations in the conterminous United States during 1950–2008, color shaded by rain category ("R-CAT") as shown in legend; b) From Dettinger et al. (2011), their Fig. 6: Contributions of precipitation during wet-season (November–April) days on which atmospheric rivers made landfall on the West Coast to overall precipitation from water year 1998 through 2008 at COOP weather stations in the western US. Inset map shows the ratio of average precipitation on the AR days (including concurrent day and following day) to climatological means for the same combination of days; c) From Ralph and Dettinger (2012), their Fig. 4: Seasonality of extreme precipitation events in the eastern versus western United States. Number of 3-day episodes achieving the highest rainfall categories, east (pink) and west (blue) of 105°W, by month of year, normalized to the number of COOP sites in each region. Two thresholds are used: light shading for R-Cat 2 (i.e., >300 mm, or approximately 12 in.), and dark shading for R-Cat 3–4 (i.e., >400 mm, or approximately 16 inches).

Figure 2. a) CFSR IWV (cm, as shaded) at 1200 UTC 03 May 2010, b) as in a) except for 1200 UTC 22 September 2003; c) IVT (kg m^{-1} s^{-1}, as shaded) at 1200 UTC 03 May 2010; d) as in c) except for 1200 UTC 22 September 2003; e) 24-h precipitation (from Livneh et al. (2013) dataset, mm, as shaded) with identified AR (white dots are AR axis points as identified by the ARDT-IVT at 1200 UTC within 24h precipitation accumulation period); f) as in e) except for 1200 UTC 22 September 2003.

Figure 3. Regional comparison of CFSR-based IWV and IVT by percentile (50, 75, 85, 90, 95, and 99th percentiles as labeled) using regions as shown in Fig. 3. a) Southeast region IWV (mm); b) Pacific region IWV (mm); c) Southeast region IVT (kg m-1 s-1) ; d) Pacific region IVT (kg m-1 s-1).

Figure 4. a) 95th percentile of January climatological value of IWV (mm; shaded as in legend); b) as in a) except for IVT (kg m^{-1} s^{-1}; shaded as in legend); c) as in a) except for July; d) as in b) except for July. All data from CFSR, 1980 - 2010. Boxes on each panel show geographic regions used for climatological averaging of integrated water vapor (IWV) and integrated water vapor transport (IVT) analysis: Pacific (western box) and Southeast US (eastern box) regions.

Figure 5. a) IWV (mm; x-axis) versus IVT (kg m^{-1} s^{-1}; y-axis) values during 196 extreme precipitation events identified in Moore et al. (2015). IWV and IVT values were derived following the method of Moore et al. (2015) and represent 24-h temporal averages (1200–1200 UTC), spatially averaged within a 5° latitude × 5° longitude box centered on the location of maximum 24-h precipitation for each heavy precipitation event. The coefficient of determination R^2 = 0.08. Dot color indicates magnitude of the 24-h average precipitation amount at all qualifying gridpoints according to legend at upper left. b) As in a) except dot color indicates magnitude of the 24-h gridpoint maximum precipitation amount according to legend at upper left.

Figure 6. Percentage of heavy precipitation events that are associated with ARs delineated by separation distance (x-axis) and time range (red/24h vs. green/48h).

Figure 7. a) Heavy precipitation event frequency by month for all heavy precipitation events (green) and larger-spatial scale heavy precipitation events (red); b) Percentage of heavy precipitation events associated with an AR by month for all heavy precipitation events (green) and

annual average/total for larger-spatial scale heavy precipitation events (red). Large spatial scale events not shown by month in (b) due to small sample sizes in some months.

Figure 8. a) Average AR width (defined by IVT = 500 kg m-1 s-1 contour) for AR events matched with heavy precipitation events (black) and AR events not matched with heavy precipitation events (gray); b) as in a) except for average IVT (in kg m-1 s-1) at all AR-identified gridpoints.

Figure 9. Season of occurrence (winter/DJF = dark blue, spring/MAM = pink, summer/JJA = gold, fall/SON = light blue) of heavy precipitation events matched with ARs within 250-km and 24-h, plotted over terrain (elevation, m, shaded as in legend). Location indicated by circle is the center point of the heavy precipitation. Circle size indicates size (in number of gridpoints) as shown in legend at lower right. Black plus signs indicate heavy precipitation events in which no AR was matched.

Figure 10: a) IVT (shaded and vectors) of extra-tropical transition of TS Nicole (2010) valid 1200 UTC 30 September 2010; b) as in a) but for IWV (mm); c) 24-h precipitation (from Livneh et al. (2013) dataset, mm, as shaded) with identified AR (white dots are AR points as identified by the ARDT-IVT at 1200 UTC 30 September 2010).

Figure 11: a) Percentage of region-wide AR detection during heavy precipitation events above (blue) and below (orange) the 5^{th}, 50^{th}, and 95^{th} heavy precipitation percentile levels; b) Percentage of region-wide AR detection during heavy (>95^{th} percentile; blue) precipitation events and lighter events (<5^{th} percentile; orange) by each month.

Figure 12. (a) ETS and (b) BIA for deterministic 24-h accumulated precipitation forecasts 12-h to 132-h lead time from the GEFS reforecast control member for the top 30 heavy precipitation

events with a matched AR (black) and top 30 heavy precipitation events without a matched AR (red).

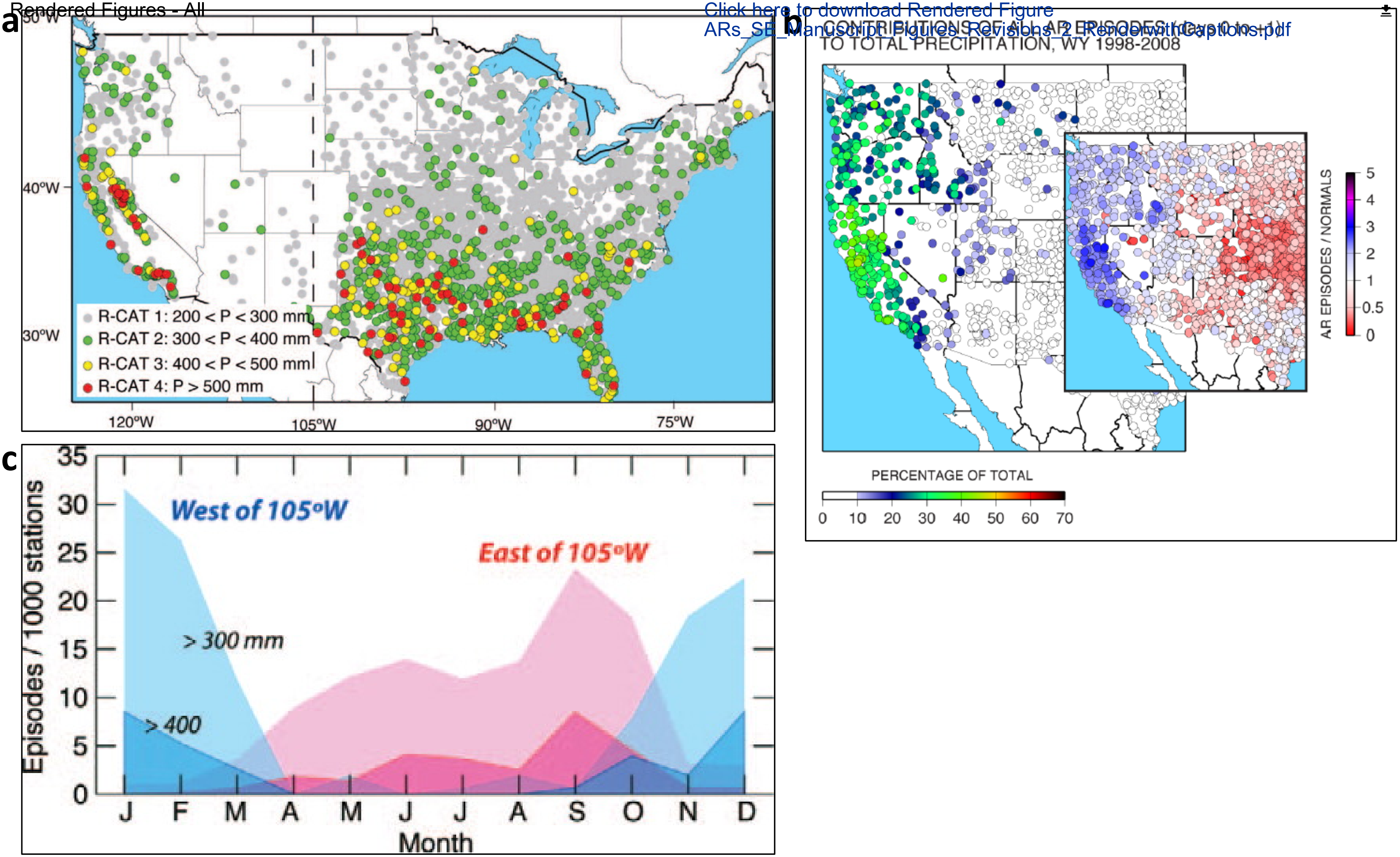

Figure 1. a) From Ralph and Dettinger (2012), their Fig. 3: Maximum 3-day precipitation totals at 5,877 COOP stations in the conterminous United States during 1950–2008, color shaded by rain category ("R-CAT") as shown in legend; b) From Dettinger et al. (2011), their Fig. 6: Contributions of precipitation during wet-season (November–April) days on which atmospheric rivers made landfall on the West Coast to overall precipitation from water year 1998 through 2008 at COOP weather stations in the western US. Inset map shows the ratio of average precipitation on the AR days (including concurrent day and following day) to climatological means for the same combination of days; c) From Ralph and Dettinger (2012), their Fig. 4: Seasonality of extreme precipitation events in the eastern versus western United States. Number of 3-day episodes achieving the highest rainfall categories, east (pink) and west (blue) of 105°W, by month of year, normalized to the number of COOP sites in each region. Two thresholds are used: light shading for R-Cat 2 (i.e., >300 mm, or approximately 12 in.), and dark shading for R-Cat 3–4 (i.e., >400 mm, or approximately 16 inches).

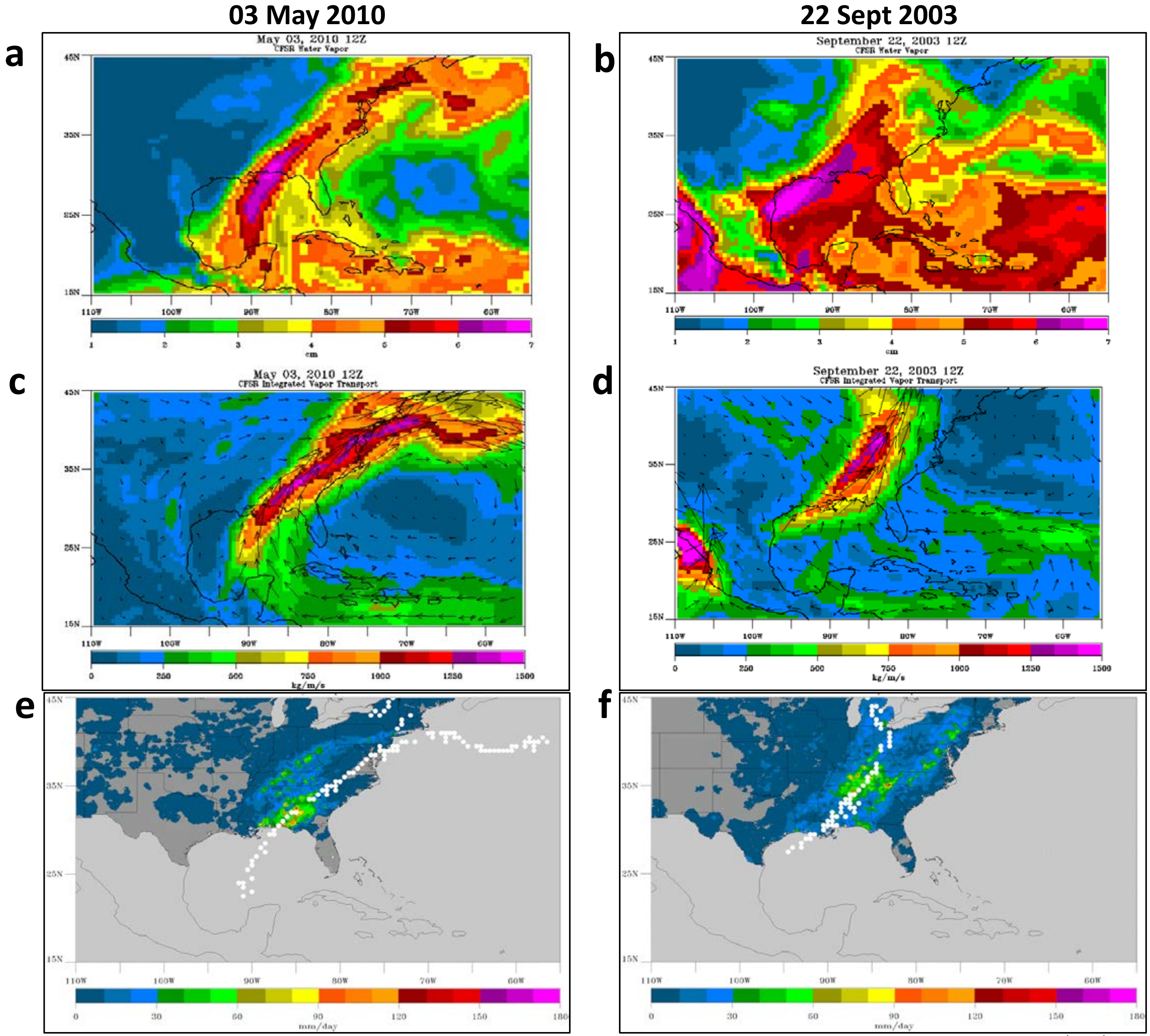

Figure 2. a) CFSR IWV (cm, as shaded) at 1200 UTC 03 May 2010, b) as in a) except for 1200 UTC 22 September 2003; c) IVT (kg s^{-1} m^{-1}, as shaded) at 1200 UTC 03 May 2010; d) as in c) except for 1200 UTC 22 September 2003; e) 24-h precipitation (from Livneh et al. (2013) dataset, mm, as shaded) with identified AR (white dots are AR axis points as identified by the ARDT-IVT at 1200 UTC within 24h precipitation accumulation period); f) as in e) except for 1200 UTC 22 September 2003.

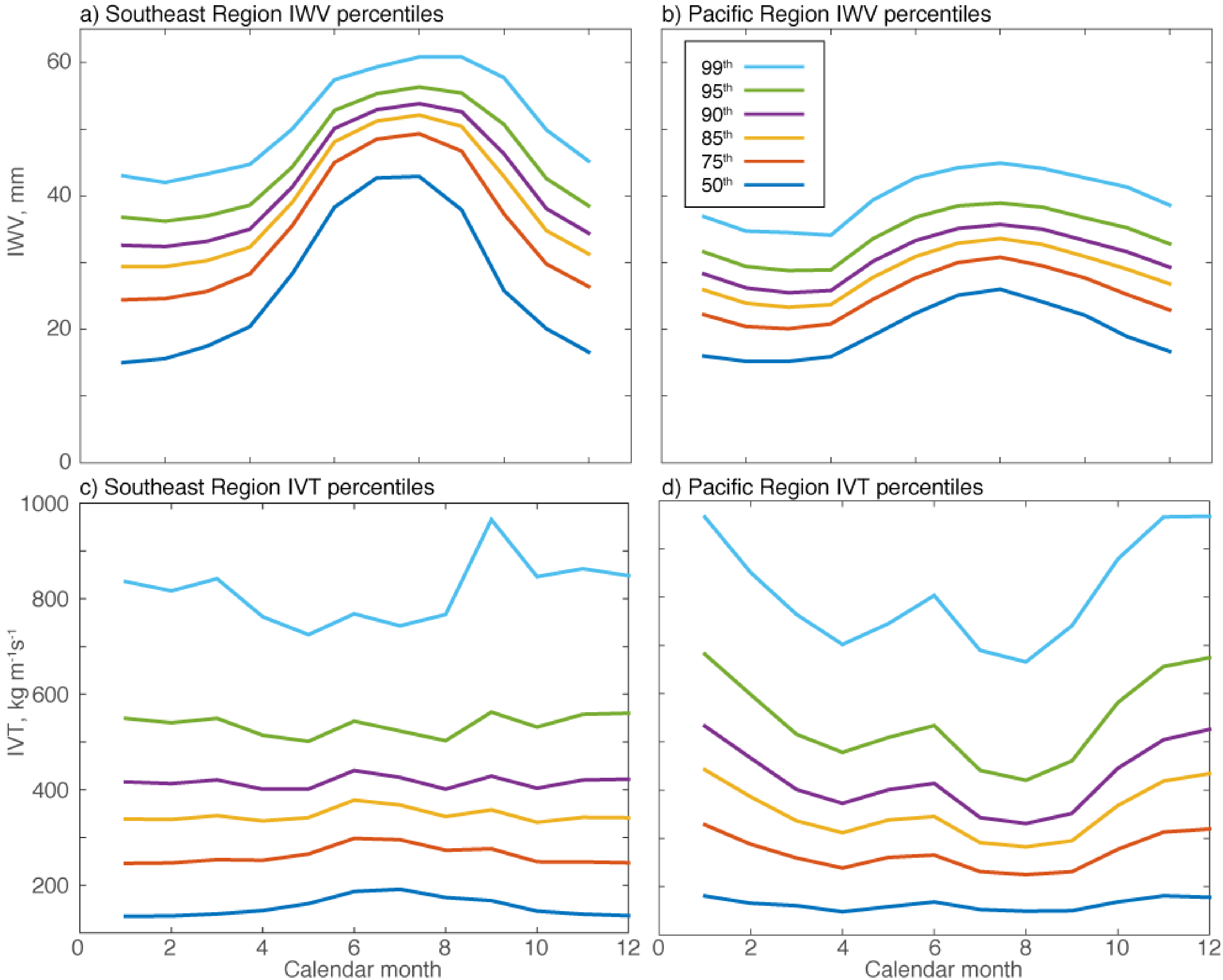

Figure 3. Regional comparison of CFSR-based IWV and IVT by percentile (50, 75, 85, 90, 95, and 99th percentiles as labeled) using regions as shown in Fig. 4. a) Southeast region IWV (mm); b) Pacific region IWV (mm); c) Southeast region IVT (kg m-1 s-1) ; d) Pacific region IVT (kg m-1 s-1).

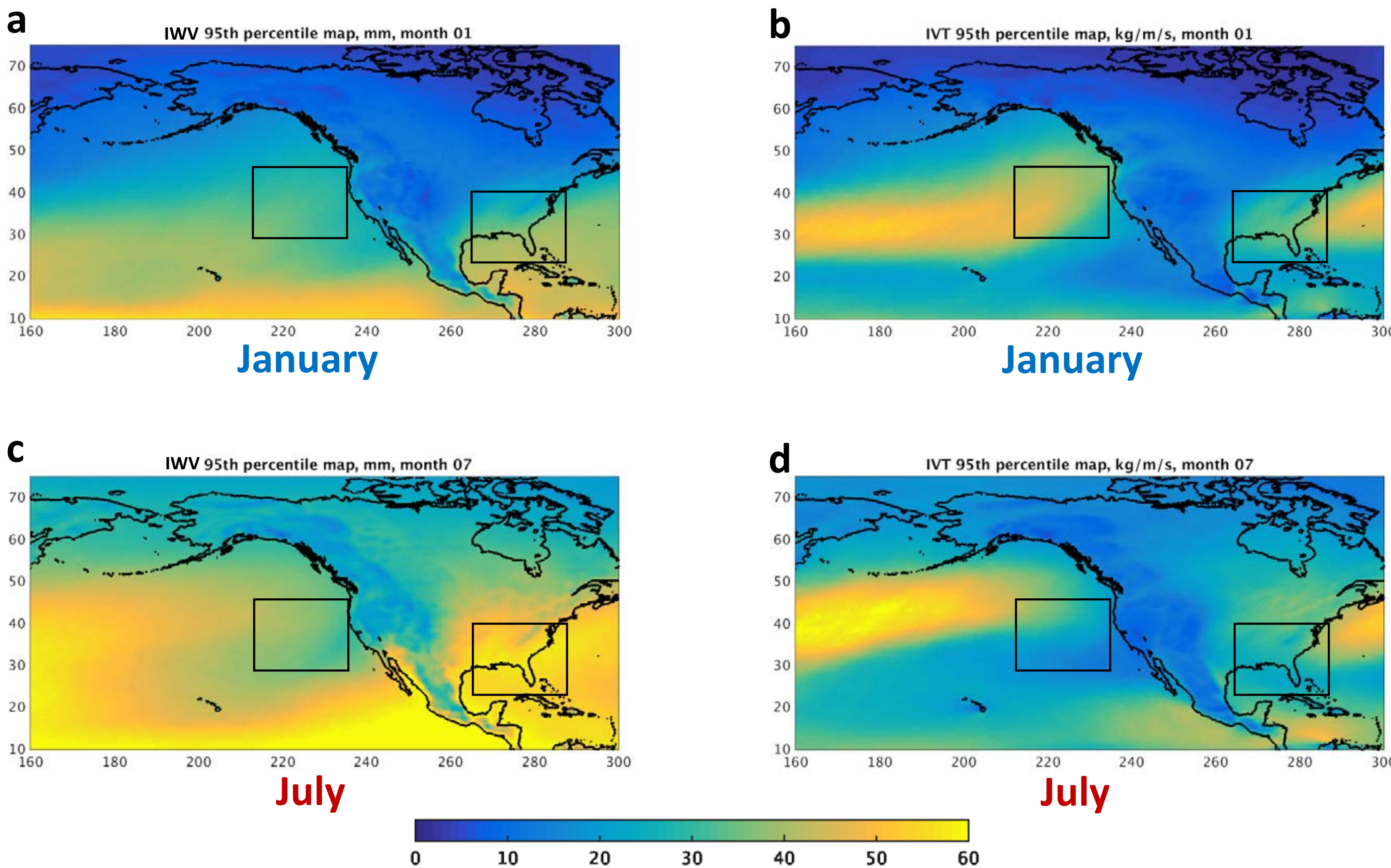

Figure 4. a) 95th percentile of January climatological value of IWV (mm; shaded as in legend); b) as in a) except for IVT (kg m-1 s-1; shaded as in legend); c) as in a) except for July; d) as in b) except for July. All data from CFSR, 1980 - 2010. Boxes on each panel show geographic regions used for climatological averaging of integrated water vapor (IWV) and integrated water vapor transport (IVT) analysis: Pacific (western box) and Southeast US (eastern box) regions.

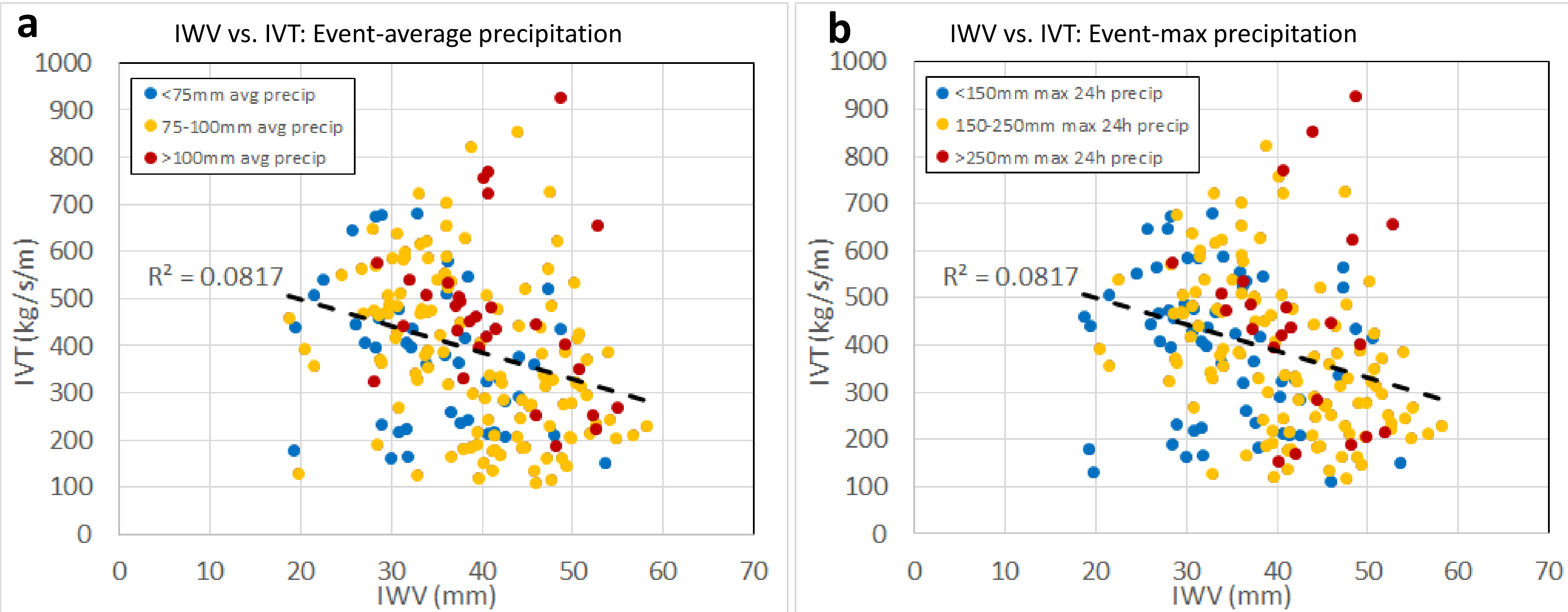

Figure 5. a) IWV (mm; x-axis) versus IVT (kg/m/s; y-axis) values during 196 extreme precipitation events identified in Moore et al. (2015). IWV and IVT values were derived following the method of Moore et al. (2015) and represent 24-h temporal averages (1200–1200 UTC), spatially averaged within a 5° latitude × 5° longitude box centered on the location of maximum 24-h precipitation for each heavy precipitation event. The coefficient of determination $R^2 = 0.08$. Dot color indicates magnitude of the 24-h average precipitation amount at all qualifying grid points according to legend at upper left. b) As in a) except dot color indicates magnitude of the 24-h grid point maximum precipitation amount according to legend at upper left.

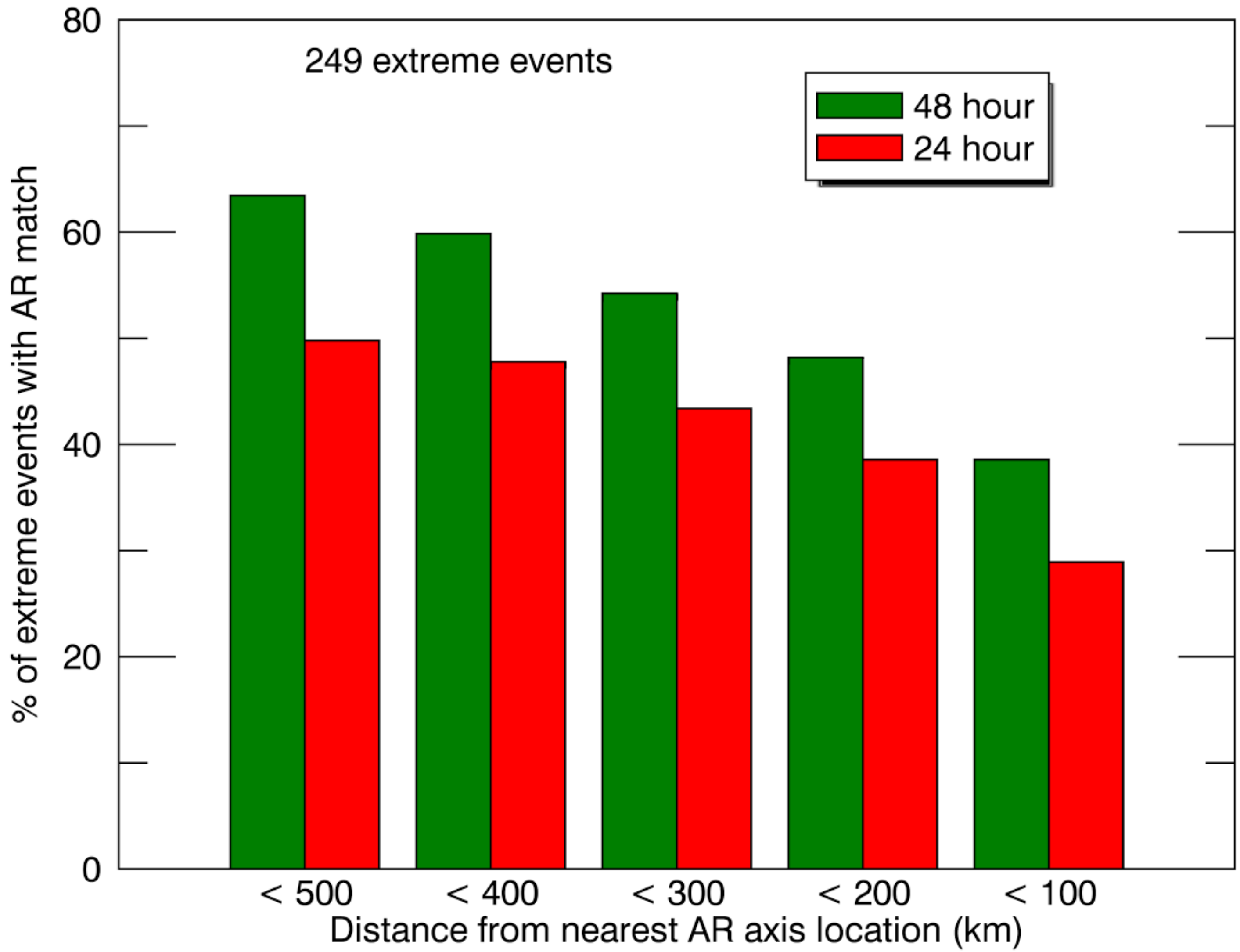

Figure 6. Percentage of heavy precipitation events that are associated with ARs delineated by separation distance (x-axis) and time range (red/24h vs. green/48h).

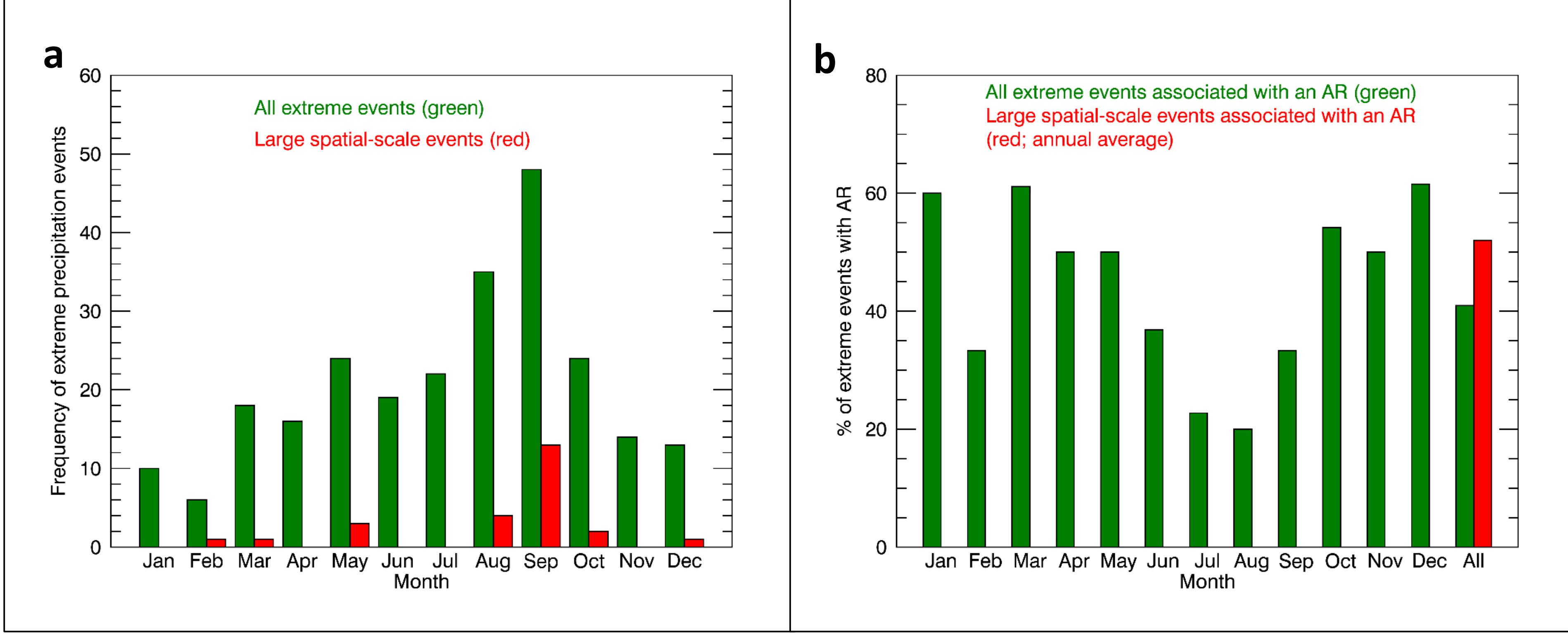

Figure 7. a) Heavy precipitation event frequency by month for all heavy precipitation events (green) and large spatial scale events (red); b) Percentage of heavy precipitation events associated with an AR by month for all heavy precipitation events (green) and annual average/total for large spatial scale events (red). **Large spatial scale events not shown by month in (b) due to small sample sizes in some months.**

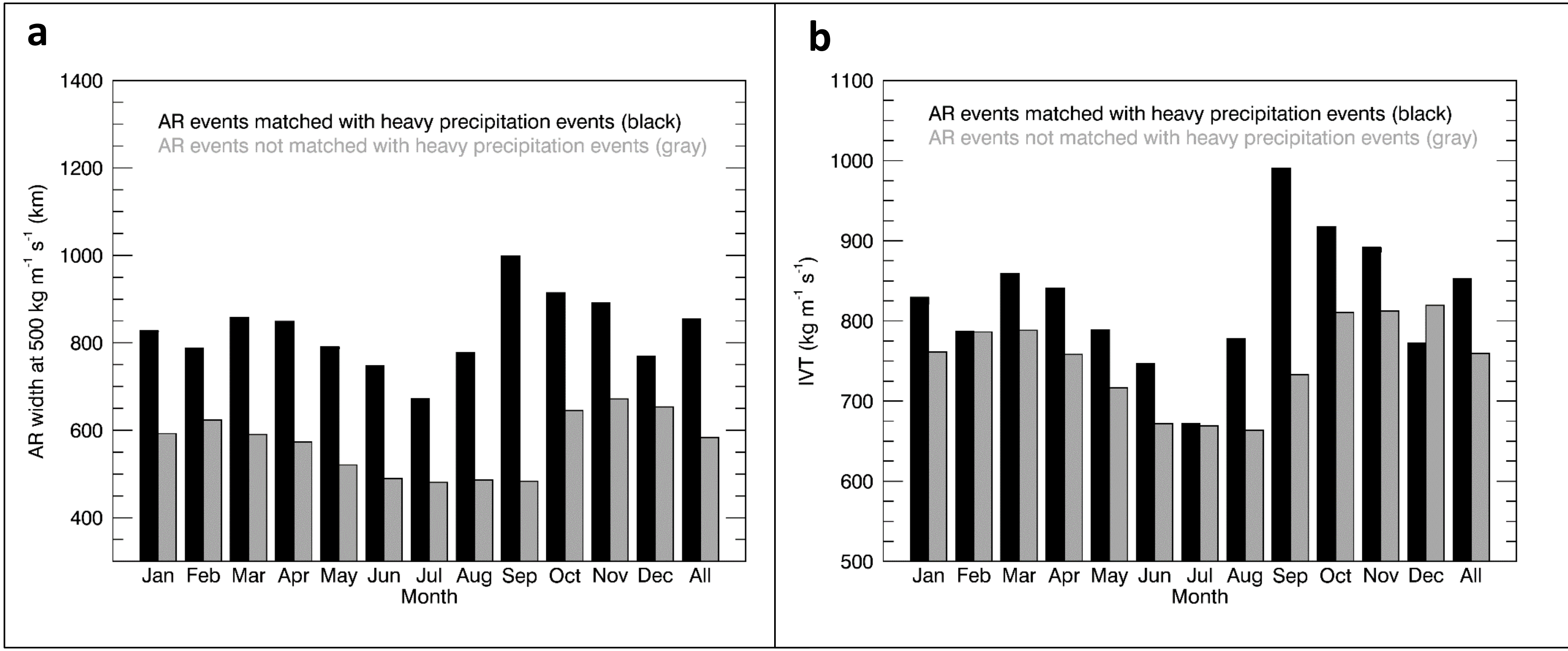

Figure 8. a) Average AR width (defined by IVT = 500 kg m-1 s-1 contour) for AR events matched with heavy precipitation events (black) and AR events not matched with heavy precipitation events (gray); b) as in a) except for average IVT (in kg m-1 s-1) at all AR-identified grid points.

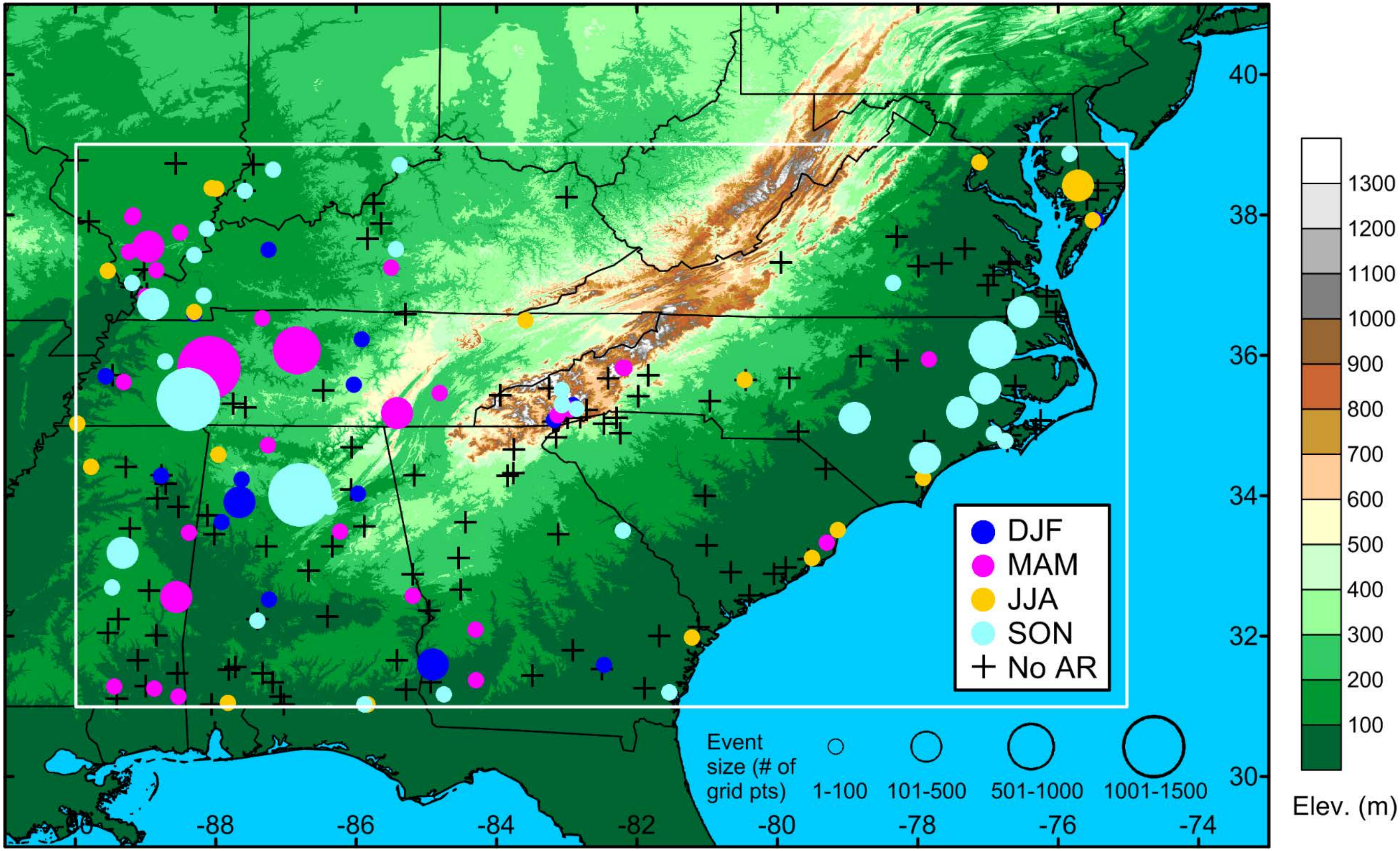

Figure 9. Season of occurrence (winter/DJF = dark blue, spring/MAM = pink, summer/JJA = gold, fall/SON = light blue) of heavy precipitation events matched with ARs within 250-km and 24-h, plotted over terrain (elevation, m, shaded as in legend). Location indicated by circle is the center point of the heavy precipitation. Circle size indicates size (in number of grid points) as shown in legend at lower right. Black plus signs indicate heavy precipitation events in which no AR was matched.

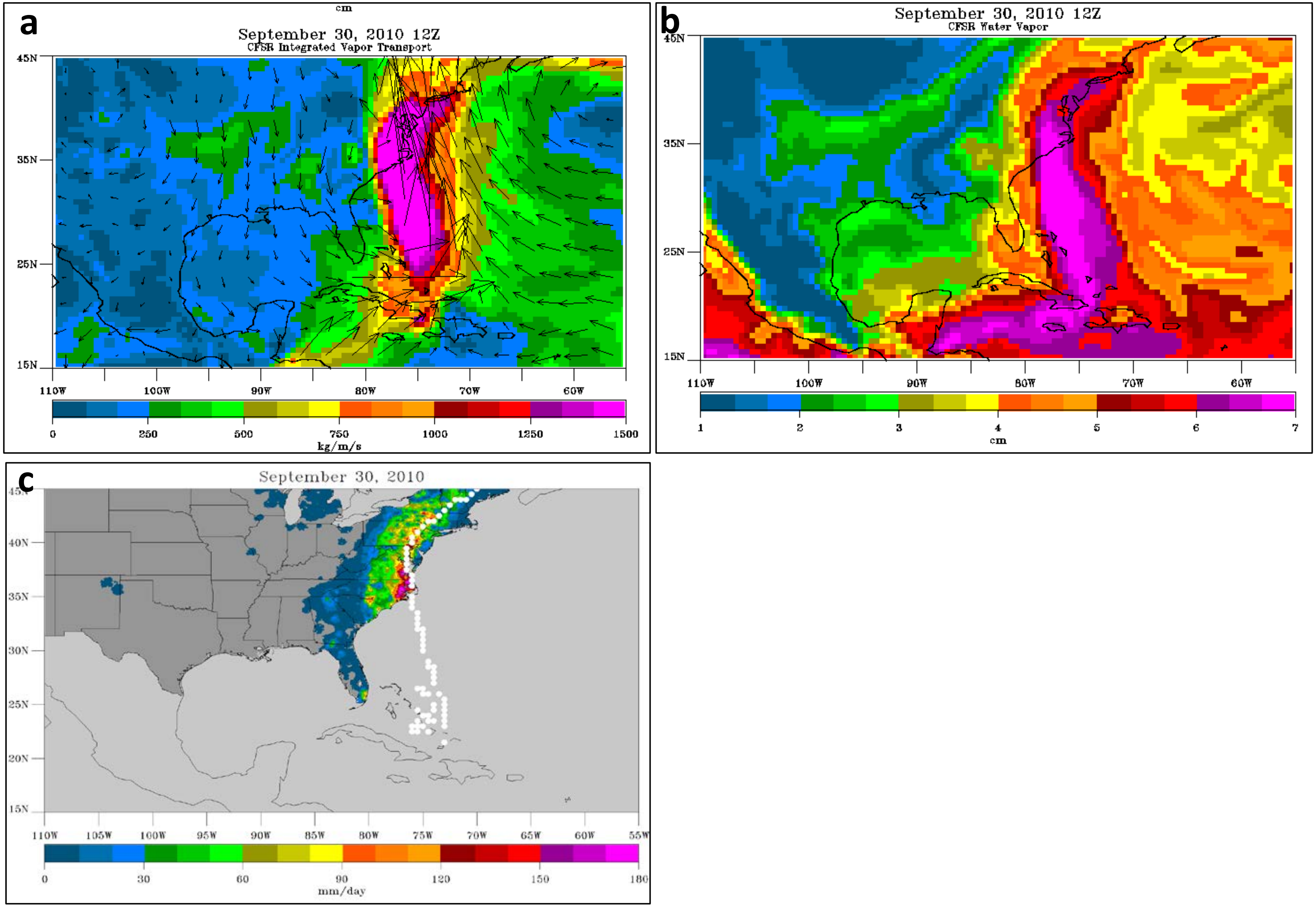

Figure 10: a) IVT (shaded and vectors) during the ET of TS Nicole (2010) valid 1200 UTC 30 September 2010; b) as in a) but for IWV (mm); c) 24-h precipitation (from Livneh et al. (2013) dataset, mm, as shaded) with identified AR (white dots are AR points as identified by the ARDT-IVT at 1200 UTC 30 September 2010).

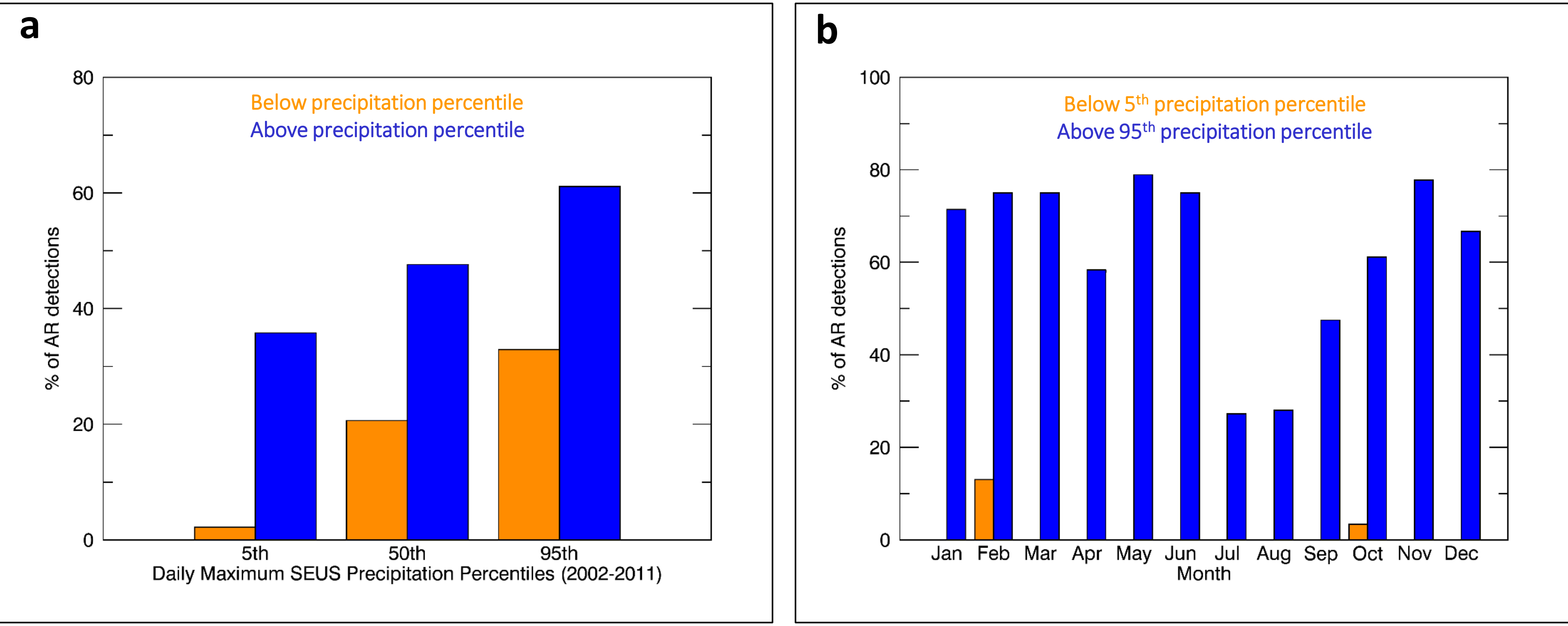

Figure 11: a) Percentage of region-wide AR detection during heavy precipitation events above (blue) and below (orange) the 5th, 50th, and 95th heavy precipitation percentile levels; b) Percentage of region-wide AR detection during heavy (>95th percentile; blue) precipitation events and lighter events (<5th percentile; orange) by each month.

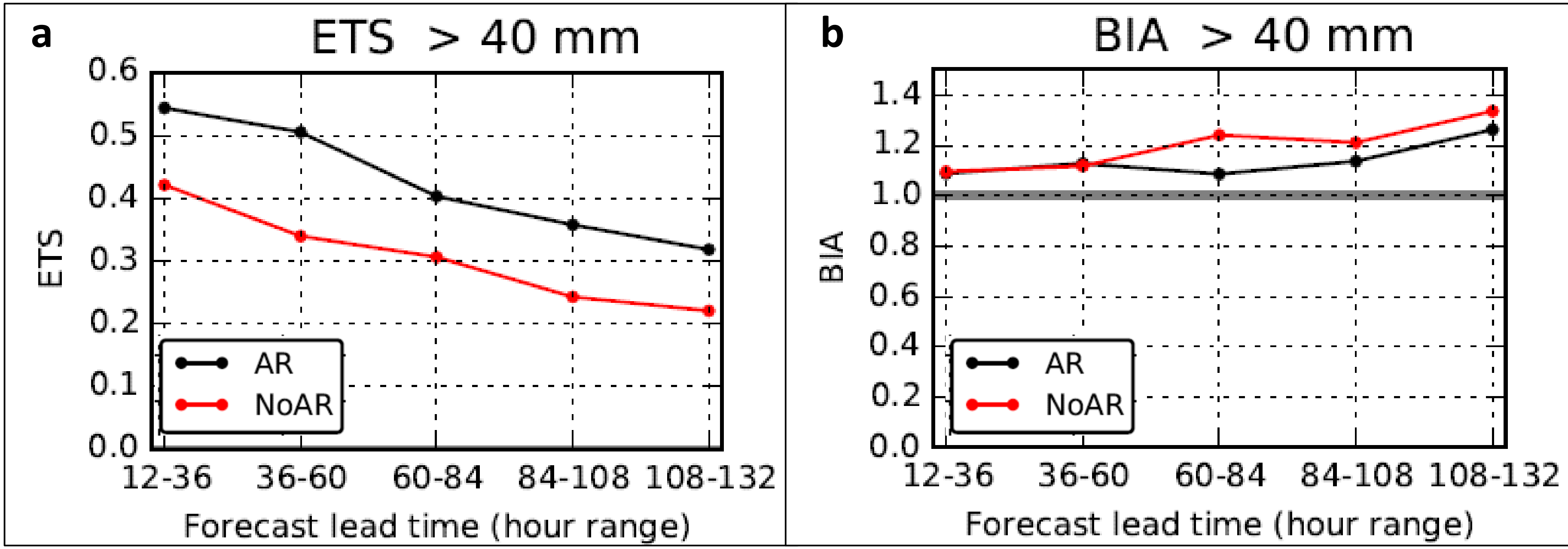

Figure 12. (a) ETS and (b) BIA for deterministic 24-h accumulated precipitation forecasts 12-h to 132-h lead time from the GEFS reforecast control member for the top 30 heavy precipitation events with a matched AR (black) and top 30 heavy precipitation events without a matched AR (red).